Optimization of Laser-Damage Resistance of Evaporated Hafnia Films at 351 nm

Introduction

Highly reflective coatings for laser applications in the ultraviolet region of the spectrum pose significant challenges since laser-damage thresholds decrease significantly as the absorption edge of the film materials is approached. Damage initiation at 351 nm for pulsed laser systems in the nanosecond-pulse regime tends to be dominated by the intrinsic absorption of the film materials, as well as defect density and the standing-wave electric-field distribution within the interference structure.[1–3] High reflectors in the near ultraviolet are typically constructed of oxides, utilizing silica as the low-index material and a refractory oxide as the high-index material. Material selection proceeds to fluorides as the wavelengths continue to become shorter and the absorption in the oxides becomes unacceptable. Silica, while somewhat challenging to evaporate, is a stable, low-absorption, high-laser-damage-threshold material that consistently outperforms the high-refractive-index component in multilayer reflectors.[1,4] The influence of the electric field distribution is quite well understood, leaving as the primary need improved high-index film materials that may be deposited with low defect density, low absorption, and high laser-damage resistance.[5,6]

Evaporated hafnia films are of particular interest for large-aperture laser applications due to the relatively high bandgap, ease of scale-up, ability to deposit uniform films, high degree of control throughout the deposition process, and relatively low intrinsic film stress.[7–10] Adjusting the deposition temperature and oxygen backfill pressure during reactive deposition may modify material parameters such as laser-damage resistance, complex refractive index, and film stress in hafnia/silica multilayers.[11–13] Furthermore, the use of hafnium metal as a source material provides a cleaner deposition than hafnium dioxide, with fewer ejected particulates, since hafnia undergoes a crystalline phase transition with a rapid change in volume while it is being heated.[14,15]

The microstructure of the deposited film is also of concern, for both mechanical and optical performance. A weak, loosely bound film structure may be environmentally and mechanically fragile, while potentially exhibiting increased tensile stress.[16–18] As roughness increases, optical scatter will also increase, reducing the efficiency of lasers incorporating such coatings.[19] In pursuing improved laser-damage resistance of the material, it is important to continue to evaluate the influence that process changes have on these other properties of the overall coating. The structure of an evaporated hafnia film tends to be quite porous, with relatively distinct zone-1 columnar growth.[20–22] This open microstructure is sensitive to the relative humidity of the use environment and is prone to tensile stress, potentially leading to cracking of the film structure. Ideally, the film microstructure could be deterministically controlled to reduce the environmental influence on film properties as well as achieve a neutral film stress in the final use environment, but there is minimal control over such properties for standard evaporated films. As porosity is increased in the film, there is a corresponding decrease in refractive index, requiring additional layers to achieve desired reflectivity specifications for reflective coatings.

A great deal of effort has been expended in determining the laser-damage mechanisms in hafnia films. The presence of "nanoclusters" of hafnium within the layers, which provide localized heating when irradiated by a laser, has been hypothesized.[23] These defects may be of the order of a few tens of atoms, leading to a reduction in laser-damage resistance as evidenced by localized initiation sites.[23] Modifications to the deposition process that avoid the formation of nanoclusters, or break existing clusters, are expected to lead to significant improvements in the laser-damage resistance of the deposited hafnia.

This effort is centered around the need to improve the laser-damage resistance of multilayer high-reflector coatings for use at a 351-nm wavelength at a 0.5-ns pulse duration. This requires the reduction, or ideally the avoidance, of nanoclusters or nanoabsorbers in the growing hafnia layers. Monolayers of hafnia are deposited for characterization by pulsed-laser-damage testing, x-ray diffraction (XRD), transmission electron microscopy (TEM), and spectrophotometry. Ideally, x-ray diffraction will be

capable of resolving the presence of any significant crystalline inclusions within the hafnia films, providing the opportunity to characterize these inclusions for size and composition. The refractive index of the film will also be characterized, in an effort to understand the impact of any changes in deposition conditions with the overall density of the film structure. Finally, multilayer high-reflector coatings will be fabricated by utilizing the established deposition process to determine the influence of the process on the performance of finished mirrors for use in a 351-nm laser.

Experimental Procedure

Depositions of hafnia films were performed in a Vacuum Process Technology (VPT) 56-in., box-type evaporation system (see Fig. 114.57). The system is cryopumped to provide a clean base vacuum of less than 3×10^{-6} Torr. The chamber is equipped with a planetary rotation system and fixed-position uniformity masks to achieve a consistent film-thickness distribution within 1% peak-to-valley. The interior of the chamber is heated using a 12-kW array of quartz heater lamps. Two Ferrotec EV-M8 electron-beam guns are utilized as evaporation sources, one equipped with six 25-cc pockets and the other a 400-cc continuously rotating pan. Deposition control is performed with an Inficon IC5 deposition controller and an array of six quartz-crystal monitor (QCM) heads, with four of the six used in a weighted average to monitor the evaporant flux from each source. This provides improved noise reduction in the thickness measurement, while averaging measurements in different regions of the chamber to minimize the effects of shifts in the vapor plume.

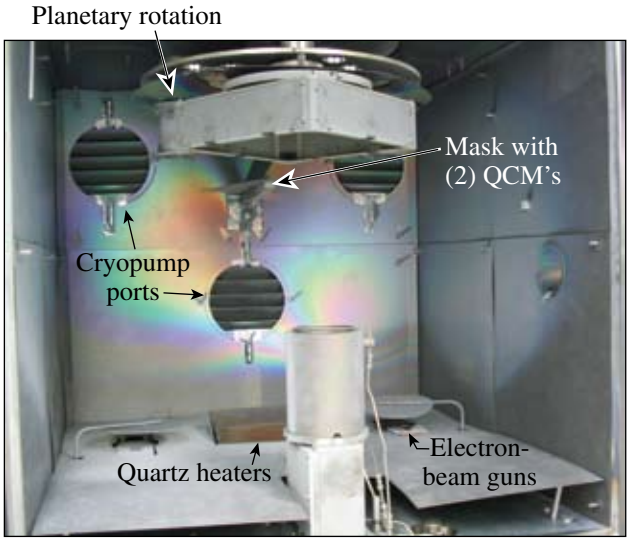

Figure 114.57
The 56-in. evaporation system used to prepare hafnia monolayers. The system uses quartz heater lamps and cryopumps and provides uniform evaporation from the electron-beam guns through the use of planetary rotation and fixed-position uniformity masks. Film-thickness control is achieved with multi-point quartz-crystal monitoring (QCM).

A cleaved-float-glass sample and a polished fused-silica substrate were placed in substrate fixtures in the planetary rotation system. The cleaved-float-glass substrate provides a virgin glass surface for more accurate determination of the laser-damage threshold, with no contaminants from cleaning or polishing processes.[4] The polished fused-silica sample is suitable for spectral measurement, x-ray diffraction, or electron microscopy. A shutter system installed on the planet made it possible to load four such pairs of substrates into the system, while only one pair is exposed at any given time. As a result four different sets of deposition conditions can be tested for each pumping cycle of the chamber.

The six-pocket electron-beam gun was loaded with 99.9%-purity hafnium metal supplied by Aran Isles. A monolayer of hafnia, with a nominal layer thickness of 177 nm, was deposited on each pair of substrates. The deposition rate was varied for each value of the oxygen backfill pressure, as outlined in Table 114.I, while the substrate temperature was maintained at 200°C for all depositions.

Measurements of Deposited Layers

The performance of the hafnia film was evaluated relative to three primary concerns: spectral/photometric performance, film stress, and laser-damage resistance. Changes in material properties were evaluated based on differences in refractive index, porosity, and crystallinity, as well as imaging of the film structure. The presence of different material phases and inclusions is of particular interest since such differences may significantly impact the laser-damage resistance of the material. Further evaluation of the material properties of the coating, such as relative elemental content or bonding structure, may be pursued in future work but was not undertaken at this time. The influence on film stress will be studied in the future for deposition conditions that yield films with sufficiently high laser-damage resistance.

First, spectral measurements were performed on all fused-silica samples at approximately 40% relative humidity using a Perkin–Elmer Lambda 900 spectrophotometer operating in a normal-incidence transmittance configuration. The transmittance measurements for the coated samples are shown in Fig. 114.58.

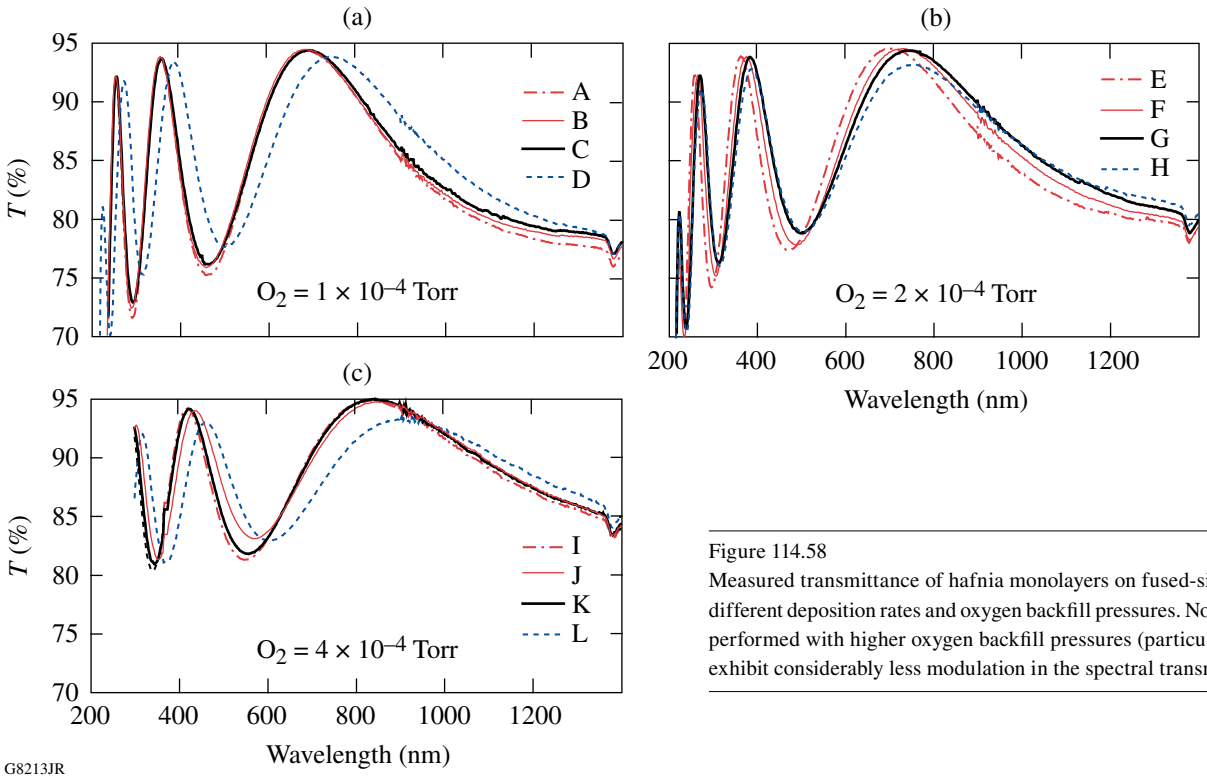

Figure 114.58
Measured transmittance of hafnia monolayers on fused-silica substrates for different deposition rates and oxygen backfill pressures. Note that depositions performed with higher oxygen backfill pressures (particularly samples I–L) exhibit considerably less modulation in the spectral transmission data.

Table 114.I: Sample identifiers A–N are assigned to substrates coated at one of six different deposition rates while using one of three oxygen backfill pressures.

Sample	O_2 Backfill Pressure (Torr)	Deposition Rate (Å/s)
A	1×10^{-4}	1.2
B	1×10^{-4}	0.9
C	1×10^{-4}	0.6
D	1×10^{-4}	0.3
E	2×10^{-4}	1.2
F	2×10^{-4}	0.9
G	2×10^{-4}	0.6
H	2×10^{-4}	0.3
I	4×10^{-4}	1.2
J	4×10^{-4}	0.9
K	4×10^{-4}	0.6
L	4×10^{-4}	0.3
M	2×10^{-4}	0.1
N	2×10^{-4}	0.2

All of the samples were characterized for their laser-damage resistance at 351 nm, using a 0.5-ns pulsed laser in a standard testing procedure.[23] Samples were tested in both 1:1 and *N*:1 configurations, with multiple threshold measurements used to establish a mean and standard deviation for each sample. Results are shown in Fig. 114.59.

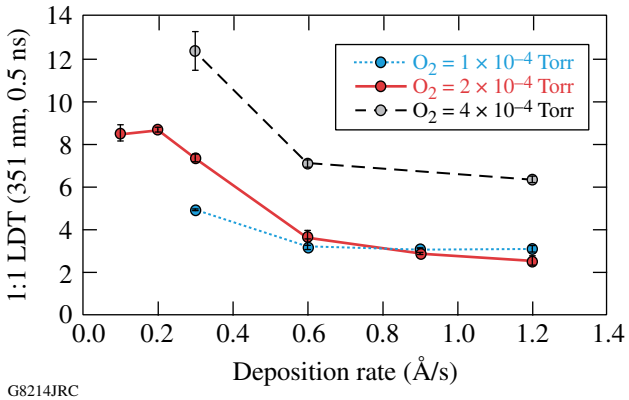

Figure 114.59
Measured laser-damage resistance of hafnia monolayers (as a function of deposition rate) at 351 nm and 0.5-ns pulse length, tested in 1:1 mode. Note the strong dependence on O_2 backfill at low deposition rates, with the slowest depositions and the greatest O_2 backfill leading to the highest laser-damage thresholds.

To better understand the material changes in the hafnia, samples were prepared for cross-section TEM, to provide high-resolution imaging of the film growth structure. Samples were prepared from multilayers consisting of hafnia layers deposited at 0.3 to 1.2 Å/s, alternated with identical silica layers, to determine the influence of changing process conditions within a single sample. Images of hafnia layers deposited at rates of 0.3 and 1.2 Å/s are shown in Fig. 114.60. Selected area electron diffraction and microdiffraction were used with a spot size of the order of 2 nm in an attempt to ascertain the presence of any crystalline nature to the hafnia material. Neither method was able to distinguish the presence of crystallites, although this may indicate that this method is not sufficiently sensitive on the thin TEM samples to properly evaluate crystalline content of these films.

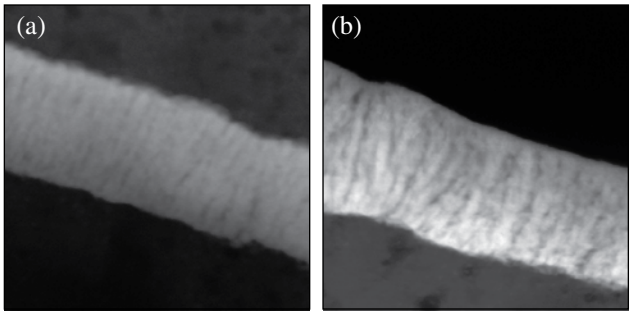

G8215JR

Figure 114.60
(a) TEM image of a layer of hafnia deposited at 1.2 Å/s in an O_2 backfill of 2.0×10^{-4} Torr. Columns are relatively distinct and perpendicular to the substrate surface. (b) TEM image of a layer consisting of hafnia deposited at 0.3 Å/s in an O_2 backfill of 4.0×10^{-4} Torr. Columns are not as distinct (more branching), and the film exhibits a greater porosity than that deposited at a higher rate. Image is in dark field, 126×126 nm.

Finally, XRD measurements of the hafnia films on samples "E" and "H" were collected using a Phillips MRD diffractometer with a Cu K_α source to evaluate the crystallinity of the hafnia structure. The coated sample was oriented in a near-grazing incidence configuration, with the incident angle $\theta = 2.2°$ and the diffracted angle 2θ incremented in steps of 0.02°, with a 13-s integration time at each position. The resulting scans are shown in Fig. 114.61.

Analysis of Hafnia Performance

The spectral transmission measurements of all of the samples in Fig. 114.58 were analyzed by fitting the measured data to a Sellmeier dispersion relationship, given by[24]

$$n^2(\lambda) = A_0 + \frac{A_1 \lambda^2}{\lambda^2 - A_2}, \quad (1)$$

where n is the wavelength-dependent real part of the index of refraction, λ is the wavelength, and A_i are the calculated constants allowing the experimental data to be fit. The refractive-index data and film thickness can be used to directly determine the theoretical transmittance of the coating by any of the standard film performance calculations or software.[24] The real part of the refractive indices determined for each of the samples is depicted in Fig. 114.62. Reducing the deposition rate decreases the real refractive index, while an increase in the oxygen backfill pressure further decreases the real refractive index. This decrease in refractive index indicates a change in the density of the film, which corresponds to an increase in film porosity. This may be experimentally observed by changes in the mechanical stability of the material and the influence of relative humidity on the film's optical thickness, which increases for highly porous films.

Results of the laser-damage testing indicate two primary features of interest. First, there is a distinct increase in the laser-damage threshold as the deposition rate is decreased. This was explored further for deposition rates below 0.3Å/s for a backfill of 2.0×10^{-4} Torr. Deposition rates of 0.2 and 0.1Å/s exhibited damage thresholds within the measurement

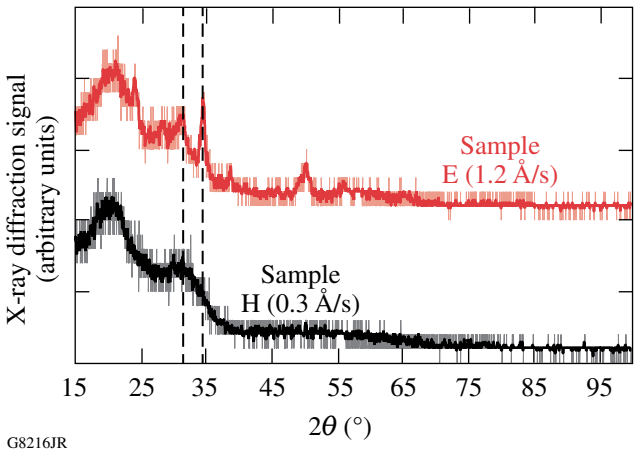

G8216JR

Figure 114.61
X-ray diffraction analysis of hafnia films deposited on silica substrates. Samples were measured in a grazing-incidence configuration, with $\theta_{incident} = 2.2°$ and 2θ incremented in steps of 0.02°, with a 13-s integration time at each position. The signal is background subtracted and smoothed with a boxcar average to clarify the diffraction peaks. As the deposition rate is increased, there is a clear increase in the crystalline signature for the film.

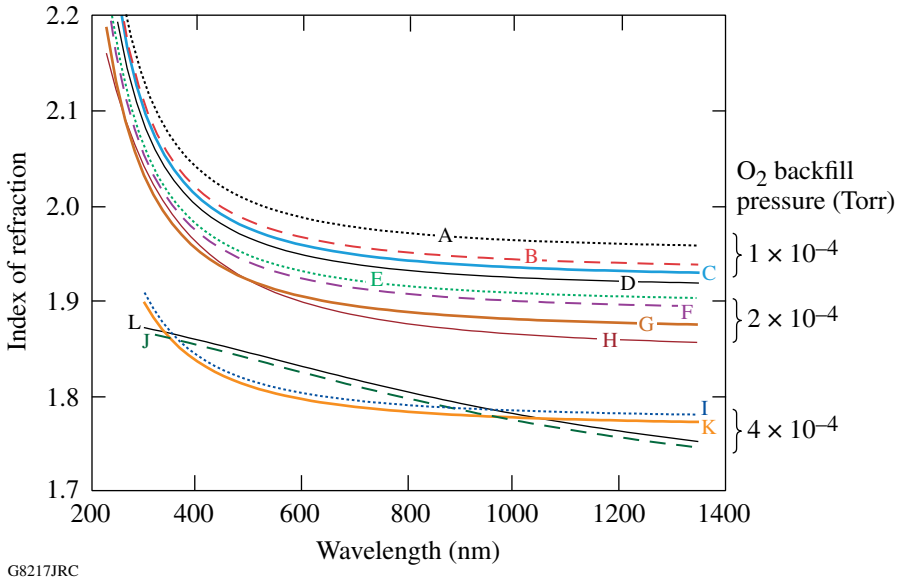

Figure 114.62
Modeled refractive indices for each of the hafnia-coated samples indicate a dependence on O_2 backfill and deposition rate. An increase in the O_2 backfill significantly reduces the hafnia refractive index, while a decrease in the deposition rate provides a lesser reduction in refractive index. Samples prepared with a backfill pressure of 4.0×10^{-4} Torr appear to have an abnormal dispersion curve, with a relatively poor fit to the Sellmeir function. This is likely due to the presence of scatter at shorter wavelengths, which also reduces transmittance.

uncertainty of each other, indicating that further decreasing the rate below 0.2 Å/s is not beneficial. Second, the laser-damage resistance at higher deposition rates is independent of the oxygen backfill pressure for the two "typical" backfill pressures (1×10^{-4} and 2×10^{-4} Torr), but a high oxygen backfill pressure of 4×10^{-4} Torr provides a substantial benefit. This likely indicates that the reduction in damage resistance at high deposition rates is not due to oxygen/hafnium adatom arrival ratios, and a resulting improvement in film stoichiometry, but some other effect of the relative deposition rates, such as film density. Hacker *et al.* argue that oxygen in excess of that needed for stoichiometric oxides benefits laser-damage resistance by increasing film porosity due to increased evaporant flux collisions with oxygen that may provide a mechanism for additional oxygen incorporation in the film.[3] This excess oxygen influences the behavior of absorptive regions in the film undergoing heating during laser interactions, as well as during recrystallization and oxidation/reduction reactions. It may saturate regions susceptible to damage, providing excess oxygen during melting and cooling, and significantly increasing the probability of formation and preservation of stoichiometric material.

Conversely, laser-damage resistance at very low deposition rates depends significantly on oxygen backfill pressure, denoting the absence of this other effect. It is suggested that this difference in laser-damage resistance is due to the presence, or lack thereof, of nanoclusters of hafnium metal (or oxide) deposited within the film. As the deposition rate is increased, the hafnium source must be heated more aggressively with a higher electron-beam current. This added energy increases the probability of ejecting very small solid particulates from the source, creating defects that will limit the laser-damage resistance. The laser-damage threshold appears independent of oxygen backfill for rates in the 0.6 to 1.2 Å/s range, except for the highest backfill pressure of 4×10^{-4} Torr, where there is a dramatic improvement. The reason for this notable improvement is not known but may relate to the interaction of the nanocluster during formation or in the surrounding film structure with the available oxygen. Further investigation is necessary to better understand this phenomenon. As the deposition rate is decreased, and the presence of these nanocluster defects is reduced or eliminated, the absorption in the film becomes the limiting damage criterion and the presence of additional oxygen further improves the film stoichiometry.

XRD Analysis

To verify the potential presence of nanoclusters or other inclusions within the hafnia film, two of the monolayers were characterized using XRD. It was expected that the nanoclusters would exhibit the crystalline nature of the hafnium source material or would be oxidized like the hafnium dioxide film, so these signatures were sought in the diffraction patterns. The size of any crystallites present may be determined based on the peak broadening given by Scherrer's equation:[25]

$$t = \frac{0.9\lambda}{B\cos\theta_B}, \tag{2}$$

where t is the crystallite size, λ is the wavelength of the x-ray illumination, B is the width of the diffraction peak in radians,

and θ_B is one-half the diffracted angle ($2\theta_B$) of the x-ray radiation. The diffraction patterns of samples E and H are shown in Fig. 114.61.

The first goal in evaluating the films with XRD is to detect the presence of crystalline nanoclusters, but of equal importance is the identification of the phase of any film inclusions. The presence of a metal inclusion, versus an oxide inclusion, should significantly affect the absorption, thermal conductivity, and resulting influence on laser-damage resistance for the component. Samples E and H exhibit a clear difference in crystallinity, as illustrated in Fig. 114.61, although the overall magnitude of the diffraction peaks is quite low, as evidenced by the relative degree of noise surrounding the peaks. The diffraction peaks observed for sample E can be analyzed to determine the phase content in the crystalline inclusions using Philips X'Pert HighScore XRD software.[26] Peak locations clearly indicate that the crystalline phase present is hafnium dioxide, not hafnium metal.

The widths of the peaks in the scan of sample E were determined to calculate the size of the crystalline inclusions. The peak at 34.59° has a measured width of 0.47°, but this is actually a double peak as indicated in hafnia reference file 78-0049 of the ICDD database. The peak at 31.44° is a good single peak with a width of 0.96°. This leads to a calculated crystallite size of 9.7 nm, in good agreement with the maximum 10-nm inclusion size determined by thermal modeling of laser-damage morphology.[23]

Application to Mirror Fabrication

The ultimate goal of this effort is to produce a mirror with a greater ability to withstand high incident laser fluence at 351 nm. Such a mirror typically consists of alternating quarter-wave optical thicknesses of hafnia and silica, so that constructive interference will lead to greater than 99% reflectivity of the incident intensity. Previous tests of silica monolayers show that the laser-damage resistance is significantly higher than that of hafnia.[4] The highest laser-damage resistance for a hafnia monolayer in this study was achieved with the lowest deposition rate (0.3 Å/s) and high oxygen backfill pressure. In order to reduce scatter, the oxygen backfill pressure was limited to 2.0×10^{-4} Torr.

A 23-layer mirror design was established to achieve the desired reflectance at 351 nm at near-normal incidence. The spectral performance of the deposited mirror shown in Fig. 114.63 is shifted to a slightly shorter wavelength than the targeted 351-nm central wavelength.

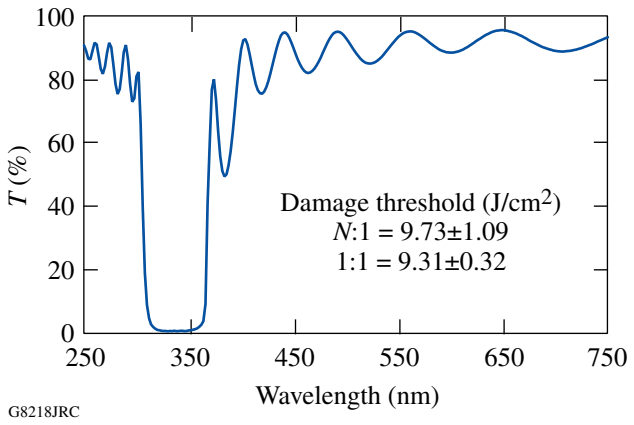

Figure 114.63
Spectral performance of a 23-layer mirror designed for near-normal incidence at 351 nm and produced by the deposition process used for sample H.

Laser-based reflectometry measurements at 351 nm indicate that the reflectivity of the mirror is 99.2% with approximately 0.5% loss due to scatter from the porous film structure. Laser-damage testing of this multilayer at 351 nm and 0.5-ns pulse length yields an *N*:1 threshold of 9.73±1.09 J/cm^2, while the 1:1 procedure results in a threshold of 9.31±0.32 J/cm^2. By comparison, hafnia/silica multilayers prepared with the standard process (hafnia deposition rate of 1.2 to 1.5 Å/s) in the past four years at LLE have yielded 1:1 damage thresholds of 1.16 to 5.64 J/cm^2, with an average threshold of 3.36 J/cm^2. Even when targeting defects in the improved mirror, the laser-damage resistance is substantially higher than that of any comparable mirror previously produced.

A 31-layer suppressed-electric-field design[5] was selected to further improve laser-damage resistance in the hafnia layers. The slow-rate deposition technique provides a great deal of flexibility in depositing the coating design since deposition rates and/or oxygen backfill pressures are readily varied for each layer deposited. More-rapid deposition may be utilized for layers interacting with lower-amplitude electric fields, providing not only faster processing, but also minimizing the number of necessary layers and decreasing the surface roughness and associated scatter. The electric-field profile of the outermost 14 layers of this design is illustrated in Fig. 114.64, indicating the deposition rates of any reduced-rate hafnia layers, all of which were deposited with an oxygen backfill pressure of 4×10^{-4} Torr. Laser-damage threshold of this coating undergoing *N*:1 testing reached 13.13±1.15 J/cm^2, while the 1:1 procedure resulted in a threshold of 12.11±0.51 J/cm^2.

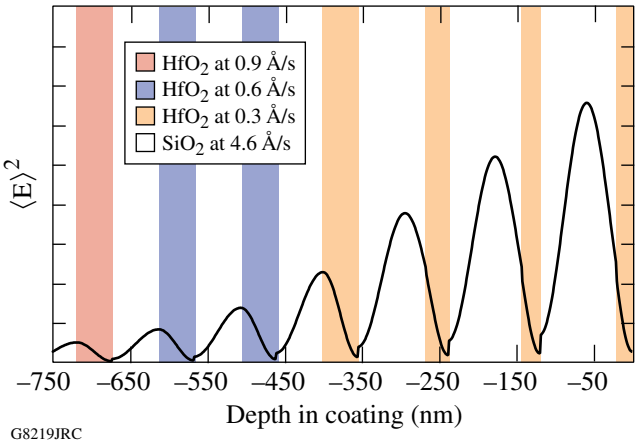

Figure 114.64
Time-averaged electric-field squared in the outer 14 layers of a hafnia/silica reflector designed for 28° incidence, *p*-polarization at 351 nm. The hafnia layer thicknesses are reduced from typical quarter-wave optical thicknesses in the outer layers to shift the peak electric fields into the more-damage-resistant silica layers. The deposition process is also adjusted to provide maximum laser-damage resistance in regions of the highest standing-wave electric-field intensity.

This testing led to the deposition of production UV transport mirrors (UVHR1 and UVHR2) for LLE's OMEGA EP Laser System. Coatings were produced on BK7 substrates with a measured *N*:1 laser-damage resistance at 351 nm and 0.5-ns pulse duration, ranging from 9 to 16.63 J/cm^2. Additionally, a strong dependence of laser-damage threshold with respect to relative humidity was noted. The measured laser-damage threshold of a single sample changed from 13.08 to 16.63 J/cm^2 as the relative humidity of the testing environment increased from 24% to 44%, respectively.

Results and Discussion

It is clear that the changes in deposition parameters of evaporated hafnia films significantly alter the refractive index, crystallinity, and laser-damage resistance. XRD makes it possible to quantitatively analyze the film structure, leading to the conclusion that higher deposition rates lead to crystalline inclusions of hafnium dioxide within the amorphous structure. The presence of smaller nanocluster inclusions of hafnium metal has been hypothesized based on laser-damage morphology, but the signature of such inclusions was not observed in the XRD measurements, nor was it apparent in the electron diffraction work. If these nanoclusters are the precursor of damage, then decreasing deposition rate must be reducing the absorption cross-section of the nanoclusters. It is likely that this results from a decrease in the mean size of the nanoclusters contained within the film, or possibly the thermal coupling of the cluster to the surrounding hafnia matrix. A sufficiently gentle evaporation, with a source temperature held very close to the evaporation temperature of the material, provides insufficient energy for the ejection of nanoclusters and improves the overall laser-damage resistance of the material.

The presence of a high oxygen backfill pressure can be expected to scatter coating molecules during transport from the source to the substrate, since the purpose of the vacuum is to increase the mean free path of the coating molecules to avoid this effect. By increasing the oxygen pressure, a greater percentage of the coating will be scattered and the film will condense with less energy at the substrate surface.[17] This energy reduction leads to a more porous film, with reduced mechanical integrity, but, as shown, the laser-damage resistance is significantly improved.

The porosity and resulting influence on the optical properties of the film may explain the relationship between relative humidity and film performance, as past experience has shown a decrease of approximately 2.7% in optical thickness for films in nominal 40% relative humidity versus purged or vacuum environments with approximately 0% relative humidity. This would lead to changes in the standing-wave electric-field profile, altering intensities within the layers and the corresponding damage thresholds. However, it is also possible that the presence of additional moisture increases the available oxygen within the film, decreasing both the hafnium-to-oxygen ratio and the absorption.[3]

It is expected that chamber geometry and e-beam sweep pattern play a significant role in the rate dependence of hafnia deposition. If the nanocluster explanation is accurate, then chamber geometries that provide a greater deposited film rate for an equivalent source heating would lead to a shifting of the inflection point in the damage graph to higher deposition rates. If the absorption and subsequent damage are primarily due to film non-stoichiometry, then higher deposition rates due to changing geometry should lead to further reductions in laser-damage resistance as oxidation becomes more incomplete. Further investigation of the film structure due to the process modifications, as well as the fundamental cause of the change in laser-damage resistance, is necessary to better understand and utilize these results.

Future Work

Reducing the deposition rate for slow film growth substantially improves laser-damage performance at 351 nm.

Further work is needed to verify the change in the size of the crystalline inclusions, using cross-section and plan-view TEM imaging. Process modifications for e-beam evaporation will be extended to deposition rates below 0.3 Å and higher oxygen backfill pressures during reactive deposition to further improve laser-damage resistance. The influence of the changing film morphology—specifically reduced density leading to potentially higher scatter in the UV—will also be explored to determine the impact on optical and mechanical properties of multilayer coatings. Texture of the film crystallinity should be investigated with XRD to better separate nucleation and film structure from the crystalline signature of film inclusions.

Conclusions

Laser-damage testing of samples processed under different deposition conditions clearly suggests that multiple factors are influencing the damage resistance of the layers. It is hypothesized that, at higher deposition rates, nanoclusters of hafnium metal are ejected from the source and embedded within the growing film, reducing the laser-damage threshold of the material. These clusters are sufficiently small that oxidation is still complete, but the presence of the crystalline inclusion in the overall amorphous structure leads to a degradation of laser-damage resistance. By reducing deposition rates, the range of cluster sizes and the corresponding absorption cross-section is also reduced, enhancing laser-damage resistance. The manipulation of the film porosity and damage resistance through the use of deposition rate and oxygen backfill pressure provides the freedom to modify only those layers interacting with the highest-intensity electric fields, where laser damage is most likely to occur. The use of this process adjustment results in significantly higher laser-damage resistance for multilayer hafnia/silica mirrors at 351 nm.

ACKNOWLEDGMENT

The authors wish to thank Malcolm Thomas (Cornell Center for Materials Research) for support in TEM sample preparation and imaging. This work was supported by the U.S. Department of Energy Office of Inertial Confinement Fusion under Cooperative Agreement No. DE-FC52-08NA28302, the University of Rochester, and the New York State Energy Research and Development Authority. The support of DOE does not constitute an endorsement by DOE of the views expressed in this article.

REFERENCES

1. A. M. Piegari, M. R. Perrone, and M. L. Protopapa, in *Sixth Conference on Optics: 2000*, edited by V. I. Vlad (SPIE, Bellingham, WA, 2001), Vol. 4430, pp. 869–881.
2. M. Reichling, A. Bodemann, and N. Kaiser, Thin Solid Films **320**, 264 (1998).
3. E. J. Hacker, H. Lauth, and P. Weissbrodt, in *Laser-Induced Damage in Optical Materials*: 1995, edited by H. E. Bennett *et al.* (SPIE, Bellingham, WA, 1996), Vol. 2714, pp. 316–330.
4. S. Papernov, D. Zaksas, J. F. Anzellotti, D. J. Smith, A. W. Schmid, D. R. Collier, and F. A. Carbone, in *Laser-Induced Damage in Optical Materials: 1997*, edited by G. J. Exarhos *et al.* (SPIE, Bellingham, WA, 1998), Vol. 3244, pp. 434–445.
5. J. H. Apfel, Appl. Opt. **19**, 1880 (1977).
6. M. L. Protopapa *et al.*, J. Vac. Sci. Technol. A **20**, 643 (2002).
7. J. B. Oliver and D. Talbot, Appl. Opt. **45** 3097 (2006).
8. J. B. Oliver, J. Howe, A. Rigatti, D. J. Smith, and C. Stolz, in *Optical Interference Coatings*, OSA Technical Digest (Optical Society of America, Washington, DC, 2001), p. ThD2.
9. J. DiJon *et al.*, in *Laser-Induced Damage in Optical Materials: 1999*, edited by G. J. Exarhos *et al.* (SPIE, Bellingham, WA, 2000), Vol. 3902, pp. 158–168.
10. C. J. Stolz, C. L. Weinzapfel, A. L. Rigatti, J. B. Oliver, J. Taniguchi, R. P. Bevis, and J. S. Rajasansi, in A*dvances in Mirror Technology for X-Ray, EUV Lithography, Laser, and Other Applications*, edited by A. M. Khounsary, U. Dinger, and K. Ota (SPIE, Bellingham, WA, 2004), Vol. 5193, pp. 50–58.
11. R. Thielsch, A. Gatto, and N. Kaiser, Appl. Opt. **41**, 3211 (2002).
12. B. Andre, J. Dijon, and B. Rafin, U.S. Patent No. 7,037,595 (2 May 2006).
13. H. Leplan *et al.*, J. Appl. Phys. **78**, 962 (1995).
14. R. Chow *et al.*, Appl. Opt. **32**, 5567 (1993).
15. C. J. Stolz *et al.*, in *Advances in Optical Interference Coatings*, edited by C. Amra and H. A. Macleod (SPIE, Bellingham, WA, 1999), Vol. 3738, pp. 318–324.
16. L. B. Freund and S. Suresh, *Thin Film Materials: Stress, Defect Formation, and Surface Evolution* (Cambridge University Press, Cambridge, England, 2003).
17. M. Ohring, *Materials Science of Thin Films: Deposition and Structure*, 2nd ed. (Academic Press, San Diego, 2002), pp. 723–730.
18. J. A. Floro *et al.*, MRS Bull. **27**, 19 (2002).
19. A. V. Tikhonravov *et al.*, Appl. Opt. **42**, 5140 (2003).
20. B. A. Movchan and A. V. Demchishin, Fiz. Met. Metalloved **28**, 653 (1969).
21. J. V. Sanders, in *Chemisorption and Reactions on Metallic Films*, edited by J. R. Anderson, Physical Chemistry, A Series of Monographs (Academic Press, London, 1971), pp. 1–38.
22. J. A. Thorton, in *Modeling of Optical Thin Films*, edited by M. R. Jacobson (SPIE, Bellingham, WA, 1988), Vol. 821, pp. 95–103.

23. S. Papernov and A. W. Schmid, J. Appl. Phys. **82**, 5422 (1997).

24. A. V. Tikhonravov and M. K. Trubetskov, OptiLayer Thin Film Software, Optilayer Ltd., http://www.optilayer.com (9 June 2005).

25. B. D. Cullity, *Elements of X-Ray Diffraction*, 2nd ed. (Addison-Wesley, Reading, MA, 1978).

26. PANalytical, Inc., Westborough, MA 01581 (see http://www.panalytical.com).